



HAL
open science

Aminobenzosuberone derivatives as PfA-M1 inhibitors: Molecular recognition and antiplasmodial evaluation

Emmanuel Salomon, Marjorie Schmitt, Elisabeth Mouray, Alastair G Mcewen, Lotfi Bounaadja, Morgan Torchy, Pierre Poussin-Courmontagne, Sarah Alavi, Céline Tarnus, Jean Cavarelli, et al.

► To cite this version:

Emmanuel Salomon, Marjorie Schmitt, Elisabeth Mouray, Alastair G Mcewen, Lotfi Bounaadja, et al.. Aminobenzosuberone derivatives as PfA-M1 inhibitors: Molecular recognition and antiplasmodial evaluation. *Bioorganic Chemistry*, 2020, 98, pp.103750. 10.1016/j.bioorg.2020.103750 . hal-02530528

HAL Id: hal-02530528

<https://hal.science/hal-02530528>

Submitted on 2 Jun 2020

HAL is a multi-disciplinary open access archive for the deposit and dissemination of scientific research documents, whether they are published or not. The documents may come from teaching and research institutions in France or abroad, or from public or private research centers.

L'archive ouverte pluridisciplinaire **HAL**, est destinée au dépôt et à la diffusion de documents scientifiques de niveau recherche, publiés ou non, émanant des établissements d'enseignement et de recherche français ou étrangers, des laboratoires publics ou privés.

Aminobenzosuberone derivatives as PfA-M1 inhibitors: molecular recognition and antiplasmodial evaluation.

Emmanuel Salomon^{a#}, Marjorie Schmitt^{a#}, Elisabeth Mouray^{b#}, Alastair G. McEwen^{c#}, Lotfi Bounaadja^b, Morgan Torchy^c, Pierre Poussin-Courmontagne^c, Sarah Alavi^a, Céline Tarnus^{a&}, Jean Cavarelli^c, Isabelle Florent^b, Sébastien Albrecht^{a*}.

a Laboratoire d'Innovation Moléculaire et Applications, UMR7042, Université de Haute-Alsace, Université de Strasbourg, CNRS, Mulhouse, France.

b Unité Molécules de Communication et Adaptation des Micro-organismes, UMR7245, Muséum National d'Histoire Naturelle, CNRS, Sorbonne Universités, Paris, France.

c Institut de Génétique et de Biologie Moléculaire et Cellulaire, UMR7104, INSERM U1258, Université de Strasbourg, CNRS, Illkirch, France.

& Current address : Laboratoire Vigne, Biotechnologies et Environnement, UPR3991, Université de Haute-Alsace, Université de Strasbourg, Colmar, France.

These authors contributed equally to this work.

Corresponding author: Sébastien Albrecht, sebastien.albrecht@uha.fr; Tel.: +33 389336714

Abstract

Aminobenzosuberone-based PfA-M1 inhibitors were explored as novel antimalarial agents against two different *Plasmodium falciparum* strains. The 4-phenyl derivative **7c** exhibited the most encouraging growth inhibitory activity with IC₅₀ values of 6.5–11.2 μM. X-ray crystal structures and early assessment of DMPK/ADME-Tox parameters allowed us to initiate structure-based drug design approach and understand the liabilities (such as potential metabolic and aqueous solubility issues) as well as identify the opportunities for improvement of this aminobenzosuberone series. It also suggested that compound **7c** should be regarded as an attractive chemical tool to investigate the different biological roles of this multifunctional PfA-M1 protein.

Keywords: PfA-M1 aminopeptidase, aminobenzosuberone inhibitors, protein crystallization, antiplasmodial activity.

1. Introduction

Despite encouraging wide-scale reduction in malaria incidence and mortality rates, malaria is still one of the most severe public health problems worldwide. It is a leading cause of death and disease in many developing countries particularly in young children. According to the WHO world malaria report 2018, there were an estimated 219 million cases of malaria and 435 000 related deaths in 2017.[1] The regular emergence of antimalarial drugs resistance threatens the global malaria control and elimination effort, especially since artemisinin-resistant strains of *Plasmodium falciparum* were observed in the Greater Mekong region.[2] There is an urgent need for the discovery of novel *Plasmodium* molecular targets and original antimalarial agents with new modes of action to combat malaria.

P. falciparum proteases have appeared as promising targets for the development of new classes of therapeutic agents against malaria. They are involved in a number of vital pathways which are essential for parasite survival: red blood cell (RBC) invasion, hemoglobin (Hb) degradation, egress.[3] Among these pathways, Hb degradation provides amino acids necessary to the metabolism and survival of the parasites inside erythrocytes[4–7], and also reduces the colloid-osmotic pressure within the host RBCs and thus preventing their premature lysis.[8,9]

One of these attractive protease targets is the *Plasmodium falciparum* M1 aminopeptidase, *PfA-M1*. This zinc-dependent metallo-aminopeptidase, belonging to the M1 family of aminopeptidases, catalyzes the cleavage of amino-acids at the N-terminus of peptides and plays a major role in the *Plasmodium* life cycle.[10–18] It has been mainly involved during asexual blood stage development in the last step of hemoglobin breakdown by hydrolyzing dipeptides into essential amino-acids. Contrary to other endopeptidases also involved in this Hb digestion, *PfA-M1* is encoded by a single copy gene (MAL13P1.56 or PF3D7_1311800) [19–21] and possesses non-redundant function with no overlapping substrate specificity with other hemoglobinas [7,22,23]. The disruption of *PfA-M1* gene has been unsuccessful until now, suggesting that this protease is important for parasite growth/multiplication.[18,19,24,25] Moreover, in *P. berghei* most proteases involved in the Hb degradation pathway could be deleted except the orthologues of *P. falciparum* falcilysin and *PfA-M1*. [26] According to omics data (Table S1), *PfA-M1* has been reported in other developmental different stages of the parasite's life cycle, as it is expressed in merozoite, gametocyte and insect stages.[15,27–35] Besides its involvement in Hb digestion, *PfA-M1* might thus also play alternative roles in RBC invasion, egress or during gametogenesis.[10,12,13,18]

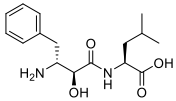
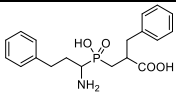
Given these results, *PfA-M1* seems to be an essential protein and hence, a very attractive validated target for the development of novel antiplasmodial drugs.[3,19,36,37] In addition,

blocking *PfA*-M1 catalytic activity with low molecular weight inhibitors is fatal for the parasite without major toxicities for the host.[16,38]

Most of the *PfA*-M1 inhibitors (Table 1) consist of tetrahedral intermediate mimics, such as the well-known aminopeptidase inhibitor bestatin **1**, or as phosphinic acid **2**, or zinc-chelating group inserted in a peptide-like scaffold, such as hydroxamic acids **3–5**. Despite demonstrating nanomolar to submicromolar activities *in vitro* on the enzyme, these compounds were usually 100 to 1000 fold less potent on *in cellulo* parasite growth inhibition assay (table 1). Only, a handful of *PfA*-M1 inhibitors (**1**, **2** and **4**) have been evaluated *in vivo* and demonstrated a reduction or suppression of the parasitaemia in murine models.[24,39] However, their frequent lack of selectivity regarding other metallo-aminopeptidase families remains problematic. Indeed, most inhibit more potently *PfA*-M17, a bimetallic aminopeptidase, which is also considered as a promising antimalarial target.[37,38,40,41] This dual activity is a valuable asset in today's malaria eradication context, but it questions the relative involvement and importance of each enzyme in the parasite biology.

In this context, our research group has previously described the development of potent and selective aminobenzosuberone-based inhibitors of APN/CD13[42–44], a human M1 aminopeptidase involved in angiogenesis and tumor metastasis.[45,46]

Recently, we reported that our scaffold **7c** demonstrated potent *in vitro* inhibitory activity and was selective for *rPfA*-M1 over *rPfA*-M17.[47] This compound was progressed to a 4-day suppressive test of Peters using a non-lethal parasite model *P.c.chabaudi* and was able to reduce the parasitaemia by 44% with a daily dose of 12 mg/kg, in four daily intraperitoneal injections, further strengthening the potential of *PfA*-M1 as a target for antimalarial research.[48]

Compound	K_i (μ M) <i>rPfA</i> -M1	K_i (μ M) <i>rPfA</i> -M17	antimalarial activity <i>in vitro</i> , <i>P.f.</i> strain, IC ₅₀ (μ M)	Toxicity	<i>in vivo</i> (<i>P.chabaudi</i>) model, parasitemia reduction
 Bestatin 1	0.19 [49]– 0.48 [38]	0.025 \pm 0.0012 [24]	FcB1, 10 Dd2, 12-21[24] D10, 11-15[24] 3D7, 3.2[49] and 8- 14[24]	ND	100 mpk, <i>b.i.d.</i> for 7 consecutive day, 34%
	0.079	0.013 \pm 0.0005	Dd2, 20-40 D10, 46-75	ND	100 mpk <i>b.i.d.</i> for 7 consecutive day, 92%

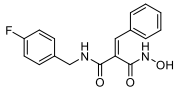
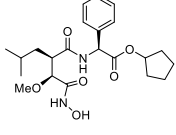
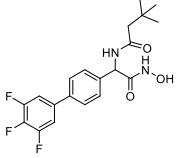
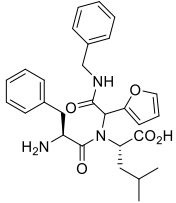
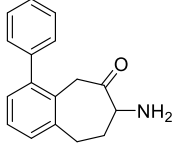
2 [24]			3D7, 24-62		
 3	0.006*[50]		FcB1, 24[50] F32, 13[50] K1, 11[51]	MRC-5, 32 μM[51]	ND
 4 [39]	1.4±0.1	0.076 ±0.022	3D7, 0.37 K1, 0.37	ND	25 mpk <i>q.d</i> for 4 consecutive day, 43%
 5 [52–54]	0.269±12	0.101±11	3D7, 0.0146±0.0008 Dd2, 0.0138±0.0005	HEK293, >20μM	ND
 6 [55]	0.4±0.1	ND	3D7, 18±7 FcB1, 16±5	HUVEC, >200μM	ND
 7c [48]	0.05±0.05	> 100	3D7, 11.2±3.4 FcB1, 6.5±2.4	L6, 141.0±12.1	12 mpk <i>q.d</i> for 4 consecutive day, 44%

Table 1 Summary of in vitro and in vivo PfA-M1 inhibitor properties. * IC50. ND no data

We report herein our initial research effort towards the identification and selection of the 4-phenyl aminobenzosuberone derivative **7c** for *in vivo* efficacy assay. We also describe the crystal structure of rPfA-M1 in complex with aminobenzosuberone derivatives **7c** and **7h**.

2. Results and discussion

2.1 Chemistry

Racemic substituted aminobenzosuberone hydrochloride derivatives **7a-j** were synthesized according to literature procedure.[43]

2.2 *In vitro* Plasmodium growth inhibition and toxicity

The encouraging results, regarding *PfA*-M1 inhibition,[47] prompted us to pursue the evaluation of this series of aminobenzosuberone scaffold as novel antimalarial agent using *in vitro* parasite growth inhibition assays. The antiplasmodial evaluation was carried out on 3D7 and FcB1 *P. falciparum* strains. The cytotoxicity of our derivatives was assessed on Vero cells (Table 2).

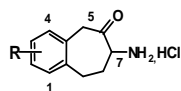
Compounds 	R ₁	R ₄	<i>In vitro</i> evaluation (μM)				SI	
			K _i <i>rPfA</i> -M1	IC ₅₀ FcB1	IC ₅₀ 3D7	CC ₅₀ Vero	<i>Pf</i> FcB1	<i>Pf</i> 3D7
Bestatin 1	-	-	0.2 - 1.5	9.0±2.1 (n=7)	8.2±1.9 (n=7)	> 300	-	-
Chloroquine			-	0.138±0.021 (n=3)	0.018±0.005 (n=7)	-	-	-
7a	H	H	15±0.07	57.3±7.4 (n=4)	64.4±10.7 (n=3)	129	2.25	2.00
7b	H	Br	0.04±0.009	22.0±9.4 (n=6)	37.3±6.0 (n=3)	21	0.95	0.56
7c	H	Ph	0.05±0.005	6.5±2.4 (n=7)	11.2±3.4 (n=5)	41 141*	6.31 21.69*	3.66 12.59*
7d	H	Fc	>50	26.9±10.0 (n=7)	24.3±2.7 (n=5)	> 500	-	-
7e	Br	H	1±0.04	17.0±4.0 (n=5)	17.9±4.9 (n=3)	21	1.24	1.17
7f	Ph	H	2±0.07	3.1±1.0 (n=5)	3.5±1.8 (n=3)	33	10.64	9.43
7g	Benzo[1,2]		15±1	95.1±9.7 (n=3)	68.9±14.6 (n=3)	300	3.15	4.35
7h	Br	Br	0.005±0.001	19.6±3.5 (n=5)	29.7±15.1 (n=5)	90	4.59	3.03
7i	Br	Ph	0.03±0.005	33.9±9.9 (n=6)	20.3±11.5 (n=5)	26	0.77	1.28
7j	Ph	Br	4±0.7	126.8±46.8 (n=3)	24.8±8.2 (n=3)	36	0.28	1.45

Table 2 *In cellulo* evaluation of racemic aminobenzosuberone hydrochloride derivatives **7a–j** on 3D7 (chloroquine susceptible) and FcB1 (chloroquine resistant) strains of *P. falciparum*, and cytotoxic evaluation on Vero cells (African green monkey kidney normal cell) using the MTT assay; * cytotoxicity and the selectivity index SI were evaluated on L6 cells; Fc = ferrocenyl; n = number of replicates. LogD_{7.4} values for all compounds are reported in Table S2.

Aminobenzosuberone derivatives inhibited *Plasmodium* parasite growth with IC₅₀ values generally ranging between 10 and 70 μM for both FcB1 and 3D7 strains. Two compounds **7c** and **7f** displayed efficacies against parasite growth *in vitro* with low micromolar IC₅₀ values, 6.5/11.2 and 3.1/3.5 μM, respectively. As a positive control, bestatin **1** displayed efficacy with IC₅₀ values of 9.0 and 8.2 μM on FcB1 and 3D7 strains respectively, which is close to previously reported values.[24,49,51] Additionally, none of the tested compounds was cytotoxic for Vero cells (IC₅₀ > 21 μM). However, they showed little selectivity of action against parasite versus mammalian cells, exemplified by a moderate selectivity index SI (ratio CC₅₀ for Vero cells / IC₅₀ for *Plasmodium* strains).

These inhibition values were similar to those previously reported for other selective PfA-M1 inhibitors, such as **3**[50,51] or **6**[55], or dual PfA-M1/PfA-M17 inhibitors, such as bestatin **1**[24,38,49] or phosphinic acid **2**[24]. Noticeable exceptions were the mixed PfA-M1/PfA-M17 hydroxamic acid-based inhibitors **4**[39] and **5**[52–54], which displayed nanomolar *in vitro* growth inhibition (< 400 nM).

Despite a large activity gap between rPfA-M1 inhibition and *Plasmodium* growth inhibition, a clear trend emerged in our results. The aminobenzosuberone derivatives showing highest K_i values on rPfA-M1 (in the micromolar range, i.e. **7a**, **7g** and **7j**) presented the least efficient growth inhibition activities against the tested parasite strains. On the other hand, compounds with good inhibition properties on the recombinant enzyme (i.e. **7b–c** and **7h–i**) showed interesting *in cellulo* results (below 30 μM). However, several exceptions must be noticed in each case. Compound **7h** was the most effective compound in inhibiting PfA-M1 catalytic activity (K_i 0.005 μM). However, it displayed poor efficacy against parasite growth *in vitro*, with IC₅₀ values ~3900-5900 times higher than those for rPfA-M1 inhibition. This significant discrepancy might be related to its poor aqueous solubility in the *in cellulo* assay media.

Despite their relatively limited inhibitory activities on rPfA-M1, compounds **7d** and even markedly **7f** were relatively potent inhibitors of *Plasmodium* growth. These unexpected results may be explained either by off-target effects for **7f** or, in the case of **7d**, by additional antimalarial activity induced by the redox-active ferrocenyl moiety leading to the formation of reactive oxygen species generated in a Fenton like reaction involving Fe³⁺/Fe²⁺. [56–58]

Interferences in MTT assays: The methylthiazolyldiphenyl-tetrazolium bromide (MTT) assay is often used to assess the cell viability of potential medicinal agents. The assay is based on the reduction of the membrane-permeable yellow tetrazolium dye by viable cells to its insoluble purple MTT-formazan product. Spectrophotometric measurement of MTT-formazan at 540 or

570 nm allows a rapid quantification of cell viability and can be used as a direct indicator of cytotoxicity of chemical compounds. However, interferences such as spontaneous reduction of MTT by the tested chemical compounds may occur, resulting in false-positive viability results, and hence giving rise to underestimated cytotoxicity values.[59]

Figure S1 indicates that compound **7c** reduces directly the MTT dye in the absence of cells. This interaction with the MTT dye should be caused by the amino-ketone functionalities. In consequence, during the MTT cytotoxicity assay with compound **7c** and potentially with the whole series of aminobenzosuberone derivatives, we should observe an increased cell viability. However, in our experiment this direct influence of the compound with the MTT reagent should be abrogated or at least mitigated by the removal of the cell growth medium and washing of the microplate wells before MTT addition.

2.3 Structural study

To gain further insight into the binding mode of this series of aminobenzosuberone inhibitors, we obtained the X-ray crystal structure of *rPfA*-M1 in complex with compound **7c** (K_i 50 nM) and **7h** (K_i 5 nM) (Table 3). Both crystals diffracted X-rays to about 1.5 Å resolution and enabled the determination of the corresponding 3D-structures (Figure 1).

	<i>rPfA</i> -M1 + 7c	<i>rPfA</i> -M1 + 7h
PDB code	6SBQ	6SBR
<i>Crystallization</i>		
Method	sitting-drop vapour diffusion	
Temperature (K)	293	
Reservoir composition	20 % PEG3350, 0.2 M di-sodium malonate	25 % PEG3350, 0.1 M BIS-TRIS propane pH 6.5, 0.2 M di-sodium malonate
<i>X-ray diffraction data collection</i>		
Diffraction Source	Proxima 1, SOLEIL	ID30B, ESRF
Detector	Dectris PILATUS 6M	Dectris PILATUS 6M
Wavelength (Å)	0.9778	0.9762
Temperature (K)	100	100
Resolution range	45.16 - 1.33 (1.378 - 1.33)	45.77 - 1.54 (1.595 - 1.43)
Space group	P 21 21 21	P 21 21 21
a, b, c (Å)	75.08, 109.24, 113.05	77.16, 109.66, 113.52
α, β, γ (°)	90, 90, 90	90, 90, 90
Mosaicity (°)	0.15 - 0.24	0.15 - 0.21
Total No. reflections	1068964 (102542)	754959 (73073)
No. of unique reflections	212163 (20854)	139879 (13623)
Multiplicity	5.0 (4.9)	5.4 (5.4)
Completeness (%)	99.71 (99.06)	99.08 (96.71)

$\langle I/\sigma(I) \rangle$	10.30 (0.54)	13.51 (0.80)
Rmerge	0.083 (2.274)	0.072 (1.983)
Rmeas ‡	0.093 (2.540)	0.080 (2.198)
Rpim	0.040 (1.111)	0.034 (0.935)
CC1/2	0.999 (0.322)	0.998 (0.432)
CC*	1 (0.698)	1 (0.777)
Overall B factor from Wilson plot (Å ²)	16.11	21.91
<i>Structure refinement</i>		
No. of reflections used in refinement	212155 (20850)	139842 (13619)
No. of reflections used for test set	10452 (1092)	6992 (682)
Rwork	0.145 (0.334)	0.143 (0.392)
Rfree	0.178 (0.356)	0.181 (0.411)
CC(work)	0.977 (0.678)	0.976 (0.637)
CC(free)	0.970 (0.618)	0.968 (0.606)
Number of non-hydrogen atoms	10052	9292
Macromolecules	8278	7963
Ligands	51	43
Solvent	1723	1286
<i>R.M.S deviations</i>		
Bonds (°)	0.006	0.005
Angles (Å)	0.84	0.88
Average B-factor (Å ²)	22.68	24.99
Macromolecules	19.94	23.01
Ligands	30.72	33.34
Solvent	35.58	37.00
<i>Ramachandran plot</i>		
Most favored (%)	97.86	98.09
Allowed (%)	2.14	1.91
Outliers (%)	0	0
Rotamer outliers (%)	0.82	0.43
Clashscore	2.65	1.23

Table 3 Crystallization, X-ray diffraction and refinement statistics. Statistics for the highest-resolution shell are shown in parentheses. ‡ R_{meas} is the redundancy-independent merging, †see [60] for definitions.

The binding mode is very similar to our previously reported **7c** / *E.coli* PepN complex (PDB 5MFS).[61] The seven-membered ring of the aminobenzosuberone core adopts a chair-like conformation and is stacked between Tyr580 and the GAMEN motif residues Val459, Gly460, Ala461 and Met462. In both complexes, the primary amine (N1) of the aminobenzosuberone core participates in a salt bridge interaction with electrostatic interactions and three hydrogen bonds with the side-chain oxygen atom of Glu319, Glu463 (of the GAMEN domain) and

Glu519. The aminobenzoerone ketone function is present in its hydrated form, with both oxygen atoms being coordinated to the zinc ion. In addition, one hydroxyl group (O1) interacts with the side-chain oxygen atom of catalytic Glu497, and the other hydroxyl of the hydrated ketone (O2) forms a hydrogen bond with the phenol moiety of Tyr580. The latter is involved in a Pi-stacking with the fused aromatic ring of the aminobenzosuberone core. Moreover, numerous hydrophobic interactions are also observed as a result of high shape complementarity between the chair-like conformation of the benzocycloheptane core and *rPfA*-M1 active site.

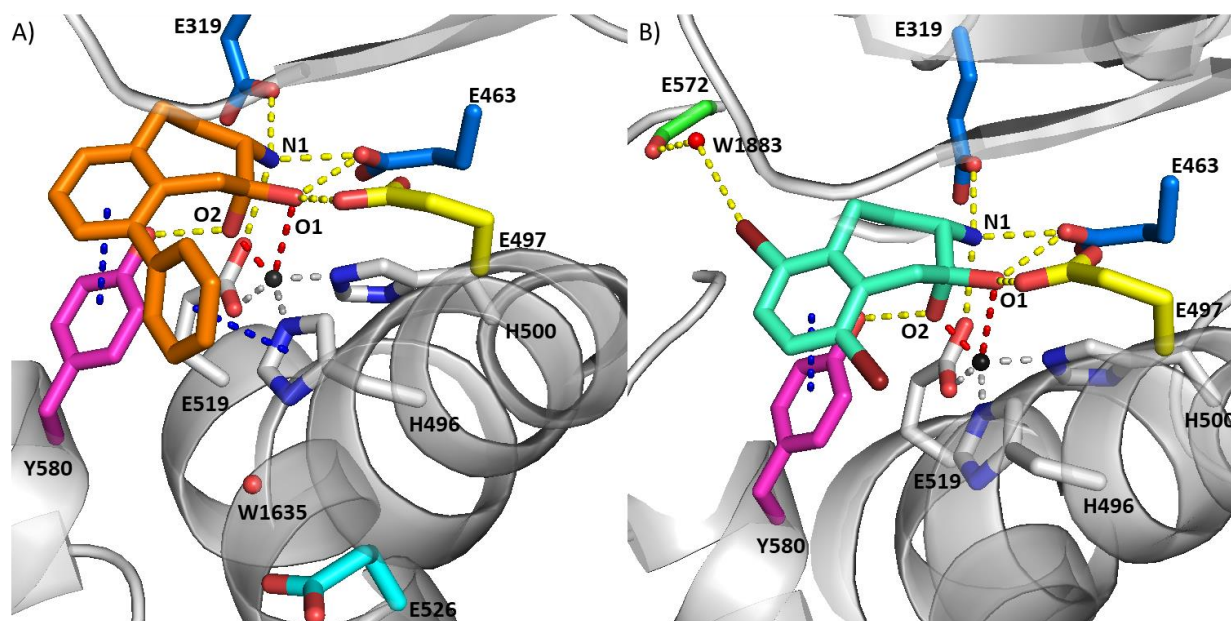


Figure 1 Crystal structure of *rPfA*-M1 complexed with (A) compound **7c** (PDB code: 6SBQ) (B) compound **7h** (PDB code: 6SBR). Compounds **7c** and **7h** are shown in orange or light green stick model, respectively. The zinc ion is shown as a black sphere, water molecule is shown as a red sphere. Pi-Pi interactions between aromatic centroids are shown as blue dashes. Hydrogen bondings are shown as yellow dashes. Interactions between the zinc ion and ligand or protein are shown as dashed red lines or dashed grey lines, respectively. The distance and angle values of these interactions are reported in Table S3. The final model and structure factors were deposited in PDB with accession code 6SBQ and 6SBR. Images generated with the PyMOL Molecular Graphics System, Version 2.0 (Schrödinger, LLC.).

An additional substituent in position 4 occupies the S1' pocket, which is lined by Thr492, Val493 and the lateral face of the guanidyl group of Arg489. The fused aromatic ring of derivative **7c** is slightly shifted towards the S1 subsite (1.2 Å compared to the aromatic core of **7h**) to accommodate its bulkier phenyl ring substituent in S1' pocket (Figure 1A). The gain in inhibitory activity of **7c/7h** versus **7a** (300 to 3000-fold) could be related to close hydrophobic interaction for the bromine substituent or Pi-Pi interaction between the additional phenyl ring

and the imidazole side chain of His496. In addition of its lipophilic properties, the bromine substituent in position 1 could also form a halogen bond with the backbone carbonyl oxygen atom of Glu572 via a bridged water molecule (W1883) in the S1 pocket (Figure 1B). Moreover, the Pi-Pi interaction between Tyr580 and the fused aromatic ring should be significantly strengthened by the presence of an electron-withdrawing bromine substituent in position 1 and/or 4.

Analysis of these structures suggests that further binding affinity improvement might be achieved by interacting with the bridged water molecule W1635, located at 3.9-4.2 Å of the 4-phenyl substituent of compound **7c**, and involved in a hydrogen bonding networks with Glu526 and the nitrogen atom of imidazole side-chain of His496 (Figure 1A). Direct interaction with the carboxylic side-chain of Glu526 might also be sought. Indeed, in some reported cases,[38] the side-chain of Glu526 points further inside the active site and interacts directly with His496, with its side-chain oxygen atom occupying the position of W49 which is expelled into the bulk solvent.

2.4 ADME *in vitro* and *in vivo*

The 4-phenyl substituted aminobenzosuberone derivative **7c** was the most promising compound, displaying a balanced inhibitory activity (*rPfA*-M1 $K_i = 50$ nM, IC_{50} 6–10 μ M on the two investigated parasite strains) and *in vitro* ADME-tox properties (Table 4).

Toxicity towards Vero cells, CC_{50} (μ M)	41.0
Toxicity towards L6 cells, CC_{50} (μ M)	141.0 \pm 12.1 (n=4)
MWT (Da)	287.78
CHI	73
$\log D_{7.4}$ calcd ^a	2.51
Human microsomal intrinsic clearance (μ L/min/mg protein)	18
kinetic solubility (μ M) ^b	151
human Plasma Protein Binding (% Bound)	83
PAMPA Permeability, P_{app} ($\times 10^{-6}$ cm/s)	7.78
CYP inhibition IC_{50} (μ M)	2C9, >10; 2D6, >10; 3A4, 5.7

Table 4 *In vitro* ADME properties of the racemic compound **7c**.

^a calculated from CHI. ^b measured from a DMSO stock solution

Compound **7c** displayed favorable profiles, with a good human microsomal stability (18 μ L/min/mg protein), moderate plasma protein binding (fraction unbound = 0.17) and favorable apparent permeability (P_{app} 7.78 $\times 10^{-6}$ cm/s). This rather low *in vitro* intrinsic clearance value should be taken with caution as it may be an artifact related to moderate CYP3A4 inhibition

(IC₅₀ = 5.7 μM). CYP inhibition may constitute a potential drug-drug interaction liability for further *in vivo* development and should be taken into consideration in optimizing this aminobenzosuberone series.

Excipient	Solubility (mM)
-	0.011± 0.003
10% Kolliphor EL	0.046 ± 0.004
15% Kolliphor HS15	0.017± 0.002
10% polysorbate 80	0.325 ± 0.012
50% PEG 400	2.8 ± 0.1
10% hydroxypropyl-β-cyclodextrin	5.5 ± 0.2

Table 5 Thermodynamic solubility of compound **7c** in PBS buffer at pH 7.4.

Although **7c** demonstrated a good kinetic solubility value, it displayed poor thermodynamic solubility at pH 7.4, suggesting that solubility could be a limiting factor for oral absorption. Significant improvement in solubility was achieved by addition of an excipient, but particularly with the formulation in which **7c** is complexed with hydroxypropyl-β-cyclodextrin (Table 4). To deliver an early *in vivo* proof of concept for this series, despite being moderately optimized, the pharmacokinetics of compound **7c** were determined in mice. Indeed, it is crucial to evaluate the pharmacokinetic properties of drug-candidate during the early phase of drug development in order to identify PK parameters requiring further improvement and optimal compound design. When dosed intravenously to female CD-1 mice at 3 mg/kg in PBS with 10% hydroxypropyl-β-cyclodextrin, the elimination half-life was short (2.2 h) with a high body clearance (43 ml/min/kg) and relatively large volume of distribution (7.4 L/kg), indicating the compound was rapidly eliminated from mouse (Table 5).

Following oral or intraperitoneal administration (3 mg/kg), compound **7c** was rapidly absorbed attaining a maximum plasma concentration of 0.8–1.3 μM at 15 min and demonstrated unfavorable AUC (1.74–2.09 μM.h) (Table 6).

PK Parameters	IV	PO	IP
clearance CL (mL/min/kg)	43	-	-
Vd _{ss} (L/kg)	7.4	-	-
half-life (start/terminal), T _{1/2} (min)	12/132	-	-
MRT (min)	170	-	-
C _{max} (μmol/L)	-	0.8	1.3
T _{max} (h)	-	0.25	0.25
AUC ₀₋₈ (μM.h)	4.25	1.74	2.09

Bioavailability F(%)	-	41	49
----------------------	---	----	----

Table 6 *In vivo* ADME properties of compound **7c** following administration of 3 mg/kg dose to female CD-1 mice (n=3 replicates). Vdss, volume of distribution at steady state. MRT, mean residence time, defined as the time for 63.2% of the administered drug molecules to be eliminated from the body; C_{max}, maximum plasma concentration; T_{max}, time to maximum concentration; AUC, area under the plasma concentration vs time curve.

Despite encouraging bioavailability (41–49%), it is noticeable, however, that C_{max} was below IC₅₀ at this dose. To achieve concentrations that are likely to be effective in PK/PD model, it is necessary to achieve a higher drug exposure (i.e., use higher doses, more frequent doses or both). For instance, assuming **7c** shows a linear pharmacokinetics, it would require at least 5 to 9-fold higher dose to reach IC₅₀. Since any dose escalation was inefficient in reducing parasitemia during our 4-day suppressive test of Peters,[48] it suggested non-linear PK behavior within the IP dose range of 12–24 mg/kg with saturation of drug absorption likely due to the poor aqueous solubility of compound **7c**.

3. Conclusion

A series of aminobenzosuberones has been investigated as novel antiplasmodial agents targeting the *Plasmodium falciparum* M1 aminopeptidase. This series was found to be highly potent and selective of rPfA-M1 with low micromolar parasite growth inhibitory activities. The co-crystal structures of **7c** and **7h** were obtained and resolved allowing us to determine the binding mode of aminobenzosuberones within the rPfA-M1 active site, paving the way for further optimization through structure-based drug design. *In vitro* and *in vivo* ADME-Tox properties for the most promising compound **7c** were determined. Despite encouraging bioavailability, solubility and clearance issues must be overcome to improve PK and efficacy of this series of aminobenzosuberone derivatives. Besides these pharmacokinetic issues, compound **7c** exhibits good membrane permeability, high potency and selectivity for PfA-M1 over other proteases and can be considered as an exquisitely selective chemical tool to decipher the precise biological functions and involvement of this multifunctional protein at different stages of *Plasmodium* life cycle.

4. Materials and methods

4.1 Biological assays

4.1.1 Cloning, expression and purification of recombinant PfA-M1

As described in literature[48], a gene encoding the cleavage site for the tobacco etch virus (TEV) protease fused to residues 192–1085 of native *Plasmodium falciparum* alanyl aminopeptidase PfA-M1 (PlasmoDB PF3D7_1311800) was synthesized by Genecust (Luxembourg), with the help of algorithms developed for optimizing, DNA sequences to improve protein expression in *Escherichia coli*. This synthetic gene was cloned into the T7 expression pET45b(+) vector (Novagen), which appended an *N*-terminal hexahistidine tag (*KpnI* and *Sall* sites).

Escherichia coli Rosetta 2 (DE3) bacteria (Novagen) were transformed with this recombinant plasmid, after its validation by Sanger sequencing (Beckman Coulter Genomics). Bacterial cultures were grown in auto-induced LB medium (Merck) supplemented with carbenicillin (50 µg/mL) and chloramphenicol (34 µg/mL), during 24 h at 25 °C, prior to bacterial extract preparation with BugBuster™ (Novagen, Darmstadt, Germany). The clarified lysate was loaded onto Ni²⁺-charged HisTrap column (GE Healthcare) equilibrated in 20 mM imidazole phosphate buffer and washed in the same buffer. Bound recombinant PfA-M1 protein was then eluted in 80 mM imidazole in phosphate buffer.

Eluted fractions were finally purified by size exclusion chromatography on a Superdex 200 10 300 (equilibrated with Tris HCl 50 mM, NaCl 200 mM, ZnCl₂ 10 µM, pH 7.4) using an Äkta purifier chromatography system (GE Healthcare Life Science, Little Chalfont, England). The SDS page gel of the different purification steps is presented in Figure S2.

4.1.2 Enzymatic Assays and Kinetic Analysis on rPfA-M1

Tests were carried out on an HP/Agilent UV-Visible diode array spectrophotometer 8453 (HP/Agilent, Santa Clara, CA, USA), at 30 °C in Tris HCl 50 mM pH 7.4, with a final DMSO concentration of 1%. Enzyme activity of rPfAM1 (10 nM) was determined by continuously measuring the release of para-nitroaniline at 405 nm with alanine para-nitroanilide as a substrate for rPfA-M1 ($K_m = 1.5$ mM). After 10 min of incubation, IC₅₀ measurements were conducted during 30 min. Initial velocities were measured with increasing concentrations of inhibitors and K_i values were determined by Dixon plots in triplicate.

4.1.3 Assays on 3D7 and FcB1 strains

In vitro antiplasmodial assays were performed on two distinct *Plasmodium falciparum* strains, FcB1 (Columbia) and 3D7 (Tanzania), that differ in their sensitivity to chloroquine, as previously described.[62] Parasites were maintained continuously in cultures on human

erythrocytes, in RPMI 1640 medium (Gibco-BRL) supplemented by 8% (v/v) heat-inactivated human serum at 37°C under and atmosphere of 3% CO₂, 6% O₂, and 91% N₂.ⁱ *In vitro* antiparasmodial activity was determined using a modification of the semi-automated microdilution technique of Desjardins et al.[63] Stock solutions of aminobenzosuberone derivative compounds (20 mM) and bestatin (Sigma-Aldrich, 30 mM) were prepared in DMSO; chloroquine (Sigma-Aldrich, 10 mM) was prepared in sterile distilled water. These were serially diluted with culture medium and introduced to asynchronous parasite cultures (1% parasitemia and 1% final hematocrite) on 96-well plates for 24 hours at 37 °C in a candle jar system (200 µl total volume per well). After 24 h, 0.5 µCi of ³H-hypoxanthin (11.1 mCi/mmol; Perkin-Elmer, France) per well were added and plates were returned to incubation at 37 °C in the candle jar system. After a further incubation of 24 h, plates were frozen / thawed and cell lysates were collected onto glass-fiber filters to be counted in a liquid scintillation spectrometer. The growth inhibition for each drug concentration was determined by comparing the radioactivity incorporated into treated cultures with the radioactivity incorporated into control cultures (without drug, but with DMSO at the same concentration) maintained on the same plates. IC₅₀s, corresponding to drug concentrations causing 50% parasite growth inhibition, were calculated from the drug concentration – response curves and the results were expressed as the mean values ± standard deviations determined from independent experiments. The DMSO concentration in the assays never exceeded 0.5%, which is the limit above which the parasite growth is affected by this solvent. Bestatin and chloroquine were used as positive controls in the assays.

4.1.3 Cytotoxicity assays on Vero and L6 cells

The cytotoxicity of aminobenzosuberone derivative compounds was estimated using the MTT method based on the ability of succinate dehydrogenase enzymes (from mitochondria) to reduce the soluble substrate 3-(4,5-dimethyl thiazol-2-yl)-2,5-diphenyl tetrazolium bromide (MTT, Sigma) into the formazan insoluble product. The assays were performed on the Vero cell line (from Monkey kidney epithelial cells) that were grown at 37 °C in the Dulbecco's Modified Eagle Medium (DMEM) supplemented with 10% (v/v) foetal calf serum. Briefly, 100 µL of cells were seeded in 96-well-plates (10 000 cells/well) and incubated overnight. Cells were treated with inhibitors dissolved in DMSO as described above, at a maximum 1% DMSO final concentration. Control wells received an equal volume of DMSO and 5-Fluorouracil (Sigma) was used as a positive control. After 72 h, the cell growth medium was removed and replaced by 100 µL of culture medium containing 10% of MTT solution (5 mg/ml), after which the plates were incubated for the next 4 h at 37 °C. Finally, 100 µL per well of SDS/DMF solution was

added and the absorbance was read after an overnight incubation. Absorbance was measured at a wavelength of 540 nm for excitation and 620 nm for emission using a microplate reader (BioTek Instruments, Inc., USA). CC_{50} , corresponding to drug concentrations causing 50% Vero cell proliferation inhibition, were calculated from the drug concentration – response curves.

Cellular cytotoxicity was also evaluated using Rat skeletal muscle cell line L6, maintained at 37°C in RPMI 1640 medium supplemented with 10% (v/v) foetal calf serum. Cells were seeded in 96-well-plates (20,000 cells/ml) and incubated for 24 hours, then, L6 cells were treated with the drug for 72 hours. After incubation, the cell growth medium was replaced by 100 μ L RPMI 1640 containing 20% (v/v) Alamar Blue (Thermofisher, France). Fluorescent viable cells were monitored after 5 hours of incubation at 37°C, at a wavelength of 530 nm for excitation and 590 nm for emission, in a FL600 luminescence spectrometer (Biotek, France). CC_{50} , corresponding to drug concentrations causing 50% L6 cell proliferation inhibition, were calculated from the drug concentration – response curves.

4.1.4 Interference in MTT assays in the absence of cells

MTT assay interference experiments with compound **7c** and a positive control (L-Glutathione) were undertaken according to Neufeld et al.[59]

Stock solutions (20 mM) of compound **7c** and L-Glutathione were made in DMSO or PBS solution (137 mM NaCl, 2.7 mM KCl, 10 mM Na_2HPO_4 , and 1.8 mM KH_2PO_4 , pH 7.4), respectively and were subsequently diluted to obtain four different concentrations (11 mM, 5.5 mM, 1.1 mM and 0.11 mM). Assays were performed in duplicate. All sample solutions were made of 5 μ L of compound **7c** and 495 μ L of PBS solution or 5 μ L of Glutathione, 5 μ L of DMSO and 490 μ L of PBS solution. Negative control sample received 5 μ L of DMSO and 495 μ L of PBS solution. To each sample solution were added 50 μ L of 12 mM MTT solution in PBS. Each sample solutions contained 0.9% DMSO final concentration. These sample solutions were incubated at 37°C for 4 h under orbital shaking at 300 rpm. Then, 425 μ L of the solution were removed, followed by the addition of 250 μ L of DMSO. The samples were further incubated at 37°C for 10 min at 300 rpm. 100 μ L of aliquots were transferred to a 96-well plate and the absorbance value was measured at 540 nm using a microplate reader (SpectraMax ID3, Molecular Devices). The data are presented as the average percent deviation from the negative control. This was calculated by the difference between the sample and control average value, divided by the control average value, and multiplied to obtain a percent value. The values are reported in Figure S1 in Supporting Information.

4.2 Crystallization

4.2.1 PfA-M1 protein for crystallization

rPfA-M1 in 20 mM Tris HCl pH 7.4, 200 mM NaCl, 10 μ M ZnCl₂ was concentrated to 5.1 mg mL⁻¹ and mixed with a 5-fold molar excess of either **7c** or **7h** (20 mM stock in DMSO) resulting in a final DMSO concentration of 1.2 %. The crystallisation experiments were carried out by the sitting-drop vapour diffusion method at 293 K using a Mosquito Crystal nanolitre dispensing robot (TTP Labtech), by mixing equal volumes (200 nL for **7c** and 400 nL for **7h**) of the complex and the reservoir solution, and equilibrating against 50 μ L of reservoir solution in 96-well 2-drop MRC crystallisation plates (Molecular Dimensions). Crystallisation conditions were screened using commercially available screens (Qiagen, Molecular dimensions, and Hampton Research), with crystals appearing in multiple conditions. The best crystal of the **7c** complex appeared in condition 60 of the PACT *premier* screen (Qiagen: 20 % PEG3350, 0.2 M di-sodium malonate), and the best crystal of the **7h** complex appeared in condition 72 of the PACT *premier* screen (Qiagen: 25 % PEG3350, 0.1 M BIS-TRIS propane pH 6.5, 0.2 M di-sodium malonate).

4.2.2 X-ray diffractometry

Crystals of *rPfAM1* in complex with compound **7c** were transferred to 35 % PEG 3350, 0.2 M sodium malonate before being mounted and flash cooled in liquid nitrogen. Crystals of *rPfAM1* in complex with compound **7h** were transferred to 25 % PEG3350, 0.1 M BIS-TRIS propane pH 6.5, 0.2 M di-sodium malonate, 10 % glycerol before being mounted and flash cooled in liquid nitrogen.

For the *rPfA-M1* / **7c** complex, data were collected at 0.9778 Å on a Pilatus 6M Hybrid Pixel Detector (Dectris) at the Proxima 1 beamline of Synchrotron SOLEIL using 0.2° oscillation range and 0.2 s exposure per image (25 % transmission). For the *rPfA-M1* / **7h** complex, data were collected at 0.9762 Å on a Pilatus 6M Hybrid Pixel Detector on the ID30B beamline of the ESRF using the MxCuBE software[64] and using 0.05° oscillation range and 0.037 s exposure per image (8.9 % transmission). All data were indexed, integrated, and scaled using XDS[65] and merged using AIMLESS[66,67] from the CCP4 suite[68], with data being processed to 1.33 Å for the **7c** complex and to 1.53 Å for the **7h** complex. Both crystals belonged to the primitive orthorhombic space group P2₁2₁2₁, with unit cell dimensions a = 75.08 Å, b =

109.24 Å, c = 113.05 Å for the **7c** complex, and a = 77.16 Å, b = 109.66 Å, c = 113.52 Å for the **7h** complex.

4.2.3 Structure solution, refinement, validation deposition and illustration

The structure of the **7c** complex was solved by molecular replacement using PHASER [69] in the PHENIX suite[70]. The structure of *PfAM1* in complex with Tosedostat (PDB ID: 4X2U)[71] was edited to remove the ligand and water molecules and used as a search model. A single solution was found with a TFZ score of 132.3 and an LLG of 28420 (unrefined: TFZ = 12.2, LLG = 21024). The asymmetric unit contains one copy of the complex, with a corresponding Matthews' coefficient[72] of 2.15 Å³ Da⁻¹ and a solvent content of 42.75 %. Refinement was performed using PHENIX[73] followed by iterative model building in COOT[74]. The structure of the **7h** complex was solved by rigid body refinement in PHENIX using the structure of the **7c** complex. The asymmetric unit contains one copy of the complex, with a corresponding Matthews' coefficient of 2.23 Å³ Da⁻¹ and a solvent content of 44.91 %.

The quality of the final refined models were assessed using MOLPROBITY[75]. Data collection and refinement statistics are given in Table 1. Structural figures were prepared with the PyMOL Molecular Graphics System, Version 2.0 (Schrödinger, LLC.) (www.pymol.org). The coordinates and structure factors have been deposited in the Protein Data Bank under the accession codes 6SBQ (**7c** complex) and 6SBR (**7h** complex).

4.3 Pharmacological properties

Determination of pharmacological properties of aminobenzosuberone derivatives **7c** was performed by TechMed^{ILL}, ESBS, Illkirch, France. Compounds are stored as 10 mM solution in DMSO at 4°C.

4.3.1 Solubility assays

Kinetic solubility was measured by diluting 20 µL of 10mM DMSO stock solution of compound in a 980 µL pH 7.4 phosphate-buffered saline (PBS) with the following composition: 137.5 mM NaCl, 2.7 mM KCl, 4.3 mM Na₂HPO₄, and 1.4 mM KH₂PO₄. Samples were shaken during 16 hours at 20-22°C. After ultracentrifugation at 15000g for 10 min at 20°C, the concentration in the supernatant was measured by a HPLC procedure on a kinetex 2.6µm C18 100A 50x2.1 mm column using a calibration line established for the compound by diluting the 10 mM DMSO stock solution to adapted concentrations. The injection volume was 20 µL, the mobile phase flow rate was 2 mL/min and the following program was applied for the elution:

0-0.1 min, 5% B; 0.1-2.6 min, 5-95% B; 2.6-3.1 min, 95% B; 3.1-3.3 min, 95-5% B and 3.3-6 min, 5% B. Solvent A was a mixture of 0.05% trifluoroacetic acid in water and solvent B was acetonitrile. The detection wavelength was 254 nm and the retention time was 1.64 min.

Thermodynamic solubility was measured by dissolving 1mg of compound in a 500 μ L pH 7.4 phosphate-buffered saline (PBS) with the following composition: 137.5 mM NaCl, 2.7 mM KCl, 4.3 mM Na₂HPO₄, and 1.4 mM KH₂PO₄ supplemented or not with 10% Kolliphor EL, 15% Kolliphor HS15, 10% polysorbate 80, 50% PEG 400 or 10% hydroxypropyl- β -cyclodextrin. Samples were shaken during 24 hours at 20-22°C. Saturation was confirmed by the presence of undissolved powder. After ultracentrifugation at 15000g for 10 min, the concentration in the supernatant was measured by a HPLC procedure on a kinetex 2.6 μ m C18 100A 50x4.6 mm column using a calibration line established for the compound by diluting the 10 mM DMSO stock solution to adapted concentrations. The injection volume was 20 μ L, the mobile phase flow rate was 2 mL/min and the following program was applied for the elution: 0-0.1 min, 5% B; 0.1-2.6 min, 5-95% B; 2.6-3.1 min, 95% B; 3.1-3.3 min, 95-5% B and 3.3-6 min, 5% B. Solvent A was a mixture of 0.05% trifluoroacetic acid in water and solvent B was acetonitrile. The detection wavelength was 254 nm and the retention time was 1.64 min.

4.3.2 CHI – logD determination

Chromatographic Hydrophobicity Indices (CHI) were determined according to an original procedure, based on a reverse phase fast HPLC gradient on a Luna C18(2) 5 μ 100A 50 x 4.6mm column. First, a solution with 10 reference compounds with known CHI values was injected onto the HPLC to generate a calibration line from their retention time ($\text{CHI} = 59.049 \cdot t_{\text{R}} - 56.021$, $R^2 = 0.9932$). The concentration of the mixture was 0.1 mg/mL for each compound and the injected volume was 5 μ L. The compound was analysed on the same system. The 10 mM DMSO stock solution was diluted to 200 μ M in CH₃CN / 50 mM ammonium acetate pH 7.4 (3:7 v/v) and 5 μ L were injected. The mobile phase flow rate was 2 mL/min and the following program was applied for the elution: 0-0.1 min, 0% B; 0.1-2.6 min, 0-100% B; 2.6-3.1 min, 100% B; 3.1-3.3 min, 100-0% B and 3.3-6 min, 0% B. Solvent A was 50 mM aqueous ammonium acetate pH 7.4 and solvent B was acetonitrile. The detection wavelength was 254 nm. The calibration line equation was used to determine the CHI values. As CHI correlates closely with LogD_{7.4} octanol/water partition coefficients, we estimated LogD_{7.4} values for the compound. Estimation of logD is calculated using the correlation equation obtained from 14 known drugs by TechMedILL ($\text{LogD}_{7.4} = 0.0515 \cdot \text{CHI} - 1.2464$, $R^2 = 0.86$).

4.3.3 Intrinsic Clearance (Cl_{int}) Determination

A 100 μ M solution was firstly prepared by diluting 10 μ L of 10 mM DMSO stock solution in 990 μ L of a water/acetonitrile mixture (1:1 v/v). This solution was then diluted 1/100 in a 100 mM phosphate buffer (pH 7.4) containing human liver microsomes (0.5 mg/mL), 3 mM $MgCl_2$ and 1 mM NADPH. 400 μ L of this solution was incubated at 37°C (initial compound concentration 1 μ M). At time zero and then at 15, 30, 45 and 60 min, two aliquots (70 μ L) of the incubation mixture were removed and diluted with acetonitrile (70 μ L) to stop the reaction. Samples were stirred for 3 min, sonicated for 3 min and centrifuged at 15000g for 5 min at 4°C. The percentage of remaining compound was determined by LC-MS/MS by measuring the area under the peak of the compound on the chromatogram using an UHPLC on a kinetex 2.6 μ m C18 100A 50x2.1 mm column coupled with a Shimadzu LCMS-8030 triple quadrupole.

1 μ L was injected. The mobile phase flow rate was 0.5 mL/min and the following program was applied for the elution: 0 min, 5% B; 0-1.2 min, 5-95% B; 1.2-1.4 min, 95% B; 1.4-1.42 min, 95-5% B and 1.42-2.8 min, 5% B. Solvent A was a mixture of 0.05% formic acid in water and solvent B was acetonitrile. The detection wavelength was 254 nm. The concentration of parent compound versus time was subsequently modelled to an exponential decay function to determine the first order rate constant for parent compound depletion (k), which was ultimately used in the estimation of microsomal clearance. Negative control was performed by replacing NADPH by a similar volume of buffer. Positive control was performed using testosterone (experimental $T_{1/2}$ 27 min, literature value 32 min).

4.3.4 PAMPA assay

A 1 mM working solution was prepared by diluting 50 μ L of 10 mM DMSO stock solution in 450 μ L of DMSO. Donor solution (50 μ M compound in 5% v/v DMSO/PBS, 1% Lucifer yellow) was prepared by diluting 1/20 the working solution in 1% v/v Lucifer yellow/PBS. An aliquot (150 μ L) of the donor solution was added to the donor plate well which contained a PVDF filter membrane (area 0.24 cm²) precoated with 5 μ L of 2% phosphatidylcholin in dodecane. The PTFE acceptor plate well was filled with 300 μ L of PBS, and the donor plate and acceptor plate were combined and incubated for 16 h at 20°C. The plates were removed from the shaker, and the acceptor sample was prepared by mixing 270 μ L of solution from the acceptor well with 130 μ L of acetonitrile. The donor sample was prepared by diluting an aliquot of solution from the donor well (20 μ L) with PBS (250 μ L) and acetonitrile (130 μ L). The T0 sample was prepared by diluting an aliquot of donor solution (20 μ L) with PBS (250 μ L) and

acetonitrile containing internal standard (130 μL). To determine the compound concentration at equilibrium, 150 μL of donor solution (50 μM compound in 5% v/v DMSO/PBS, 1% Lucifer yellow) were diluted with 300 μL PBS (pH 7.4). The prepared samples were analysed by LC-MS/MS by measuring the area under the peak (AUC) of the compound on the chromatogram using an UHPLC on a kinetex 2.6 μm C18 100A 50x2.1 mm column coupled with a Shimadzu LCMS-8030 triple quadrupole. 1 μL was injected. The mobile phase flow rate was 0.5 mL/min and the following program was applied for the elution: 0 min, 5% B; 0-1.2 min, 5-95% B; 1.2-1.4 min, 95% B; 1.4-1.42 min, 95-5% B and 1.42-2.8 min, 5% B. Solvent A was a mixture of 0.05% formic acid in water and solvent B was acetonitrile. The detection wavelength was 254 nm.

The effective permeability value (Pe) was calculated using following equation,

$$Pe = -C \ln \left[1 - \frac{AUC_A}{AUC_{eq}} \right]$$
$$C = \frac{V_D \times V_A}{(V_D + V_A) \times area \times time}$$

Similar experiments were performed in parallel with chloramphenicol and testosterone used as negative (experimental log $Pe = -6.4$, literature value -7.0) and positive (experimental log $Pe = -4.6$, literature value -4.4) permeability markers, respectively.

4.3.5 Plasma protein binding protocol- Rapid Equilibrium Dialysis (RED) Assay Conditions

Single use RED device inserts were positioned in the PTFE RED base plate. Each insert consisted of 2 chambers separated by a vertically aligned semipermeable cellulose membrane with a molecular weight cut off (MWCO) of 12 kDa. Spiking solutions of compound and warfarin were diluted in DMSO to 100 μM (10 μL of stock solution + 990 μL of DMSO). Human plasma was spiked with compound or verapamil, which served as binding positive control, to achieve final concentrations of 1 μM . The final percentage of DMSO in the plasma incubation samples was 1%. Spiked plasma (200 μL) was added to the red chamber of the RED device insert and PBS (350 μL) was added to the white chamber. The samples were allowed to dialyze for 4 hours at 37°C in an orbitaler while agitating at a rate of 250 rpm. Each sample was incubated in duplicate. At the end of the incubation, 70 μL aliquots were removed from each chamber and matrix-matched, i.e., an equal volume of PBS was added to the plasma test incubation sample and an equal volume of plasma was added to the PBS test incubation sample. Samples where protein precipitated with 350 μL acetonitrile were frozen before analysis. After thawing, the samples were vortex-mixed for 3 min and sonicated for 3 min. The samples were

then centrifuged at 15 000g for 5 min at 4°C to precipitate any proteins. The supernatants were analysed by UHPLC on a kinetex 2.6µm C18 100A 50x2.1 mm column coupled with a Shimadzu LCMS-8030 triple quadrupole using a calibration line established for the compound by diluting a 10 mM DMSO stock solution to adapted concentrations (0.05-2 µM). 1 µL of each sample was injected. The mobile phase flow rate was 0.5 mL/min and the following program was applied for the elution: 0 min, 5% B; 0-1.2 min, 5-95% B; 1.2-1.4 min, 95% B; 1.4-1.42 min, 95-5% B and 1.42-2.8 min, 5% B. Solvent A was a mixture of 0.05% formic acid in water and solvent B was acetonitrile. The detection wavelength was 254 nm. The unbound fraction was determined as the ratio of the peak area in buffer to that in plasma. Positive control was performed using verapamil (experimental F_u 10%, literature value 8%).

4.3.6 CYP inhibition

The compound (0.1–10 µM) was incubated with human liver microsomes (BD Biosciences, Switzerland) (0.05, 0.16 and 0.2 mg/mL, for 3A4, 2D6 and 2C9 inhibition assays, respectively) and NADPH (1 mM) in a 100 mM potassium phosphate buffer pH 7.4 in the presence of a cytochrome P450 isoform-specific probe substrate (diclofenac for CYP2C9, bufuralol hydrochloride for CYP2D6, and midazolam maleate for CYP3A4) in a 37 °C water bath for the appropriate incubation time (10, 30 and 15 min for 3A4, 2D6 and 2C9, respectively). The reactions were terminated by adding ice-cold acetonitrile containing an internal standard followed by vortex mixing. The samples were then centrifuged at 15 000g for 10 min at 4 °C to precipitate the microsomal proteins. After centrifugation, the supernatants were analyzed by an UHPLC on a kinetex 2.6µm C18 100A 50x2.1 mm column coupled with a Shimadzu LCMS-8030 triple quadrupole. For each isoform, a selective inhibitor (sulfaphenazole for CYP2C9, quinidine for CYP2D6, and ketoconazole for CYP3A4) was used as a positive control. The IC_{50} values were calculated by nonlinear regression analysis from the plotted remaining metabolic activity at each test compound concentration.

4.3.7 Animals

All animal experiments were carried out in accordance with the EU directive 2010/63/UE and the relevant national legislation, namely the French “décret no.2013-118, 1er février 2013, Ministère de l’Agriculture, de l’Agroalimentaire et de la forêt”. For the pharmacokinetics studies performed by TechMedILL service (ESBS, Illkirch, France), mice were housed in polycarbonate cages (PCT2L12SHT, Allentown) enriched with play tunnels throughout the experimental phase. The mice were housed in groups of nine animals during the study, under

controlled environment (22 ± 1 °C) with a relative humidity ($50 \pm 10\%$) and a normal 12 h light cycle (at 8:00 pm lights off). A standard chow diet (A04, SAFE, France) and tap water were provided ad libitum. All animal protocols done by TechMedILL service were reviewed and approved by the agriculture ministry regulating animal research in France (Ethics regional committee for animal experimentation Strasbourg, APAFIS 1341#2015080309399690).

4.3.8 *In vivo* Pharmacokinetics

Female CD-1 mice were intravenously administered a 2 mL/kg solution of **7c** (3mg/kg dose; 1.5mg/mL of **7c** dissolved in PBS solution containing 10% w/v hydroxypropyl- β -cyclodextrin). In additional studies, mice were intraperitoneally administered a 10 mL/kg solution of **7c** (3mg/kg dose; IV solution diluted 1:5 with PBS solution) or orally administered a 10 mL/kg solution of **7c** (3mg/kg dose; IV solution diluted 1:5 with distilled water). The animals were sacrificed at 5, 15 and 30 minutes, 1, 2, 4, 6, and 8 hours after administration (n=3 per time), and blood samples were collected by cardiac puncture. The plasma was separated by centrifugation and stored frozen at -80°C. 400 μ L of each plasma sample were mixed with 1 mL of acetonitrile, followed by vortex mixing for 3 min and sonication for 3 min. The samples were then centrifuged at 15 000g for 5 min at 4°C to precipitate any proteins. After centrifugation, the concentration in the supernatants were analyzed by UHPLC on a kinetex 2.6 μ m C18 100A 50x2.1 mm column coupled with a Shimadzu LCMS-8030 triple quadrupole using a calibration line established for the compound by diluting a 10 mM DMSO stock solution to adapted concentrations (0.05-2 μ M). 1 μ L was injected. The mobile phase flow rate was 0.5 mL/min and the following program was applied for the elution: 0 min, 5% B; 0-1.2 min, 5-95% B; 1.2-1.4 min, 95% B; 1.4-1.42 min, 95-5% B and 1.42-2.8 min, 5% B. Solvent A was a mixture of 0.05% formic acid in water and solvent B was acetonitrile. The detection wavelength was 254 nm. Pharmacokinetic parameters were derived from the blood concentration time curve using the non-compartmental analysis of PK Solver 2.0.[76]

Declaration of interest

The authors have declared no conflict of interest.

Acknowledgments

The support of the *Université de Haute-Alsace* and the *Ecole Nationale Supérieure de Chimie de Mulhouse* is gratefully acknowledged. We also wish to thank the *Agence Nationale de la Recherche* for its financial support (ANR-12-BS07-0020-01). The authors acknowledge the

support and use of the resources of the French Infrastructure for Integrated Structural Biology (FRISBI) ANR-10-INBS-05 and of Instruct-ERIC. This study was supported by the grant ANR-10-LABX-0030-INRT, a French State fund managed by the Agence National de la Recherche under the frame program Investissements d’Avenir ANR-10-IDEX-0002-02. We acknowledge SOLEIL (proposal 20140777) and the European Synchrotron Radiation Facility (ESRF proposal MX-1746) for provision of synchrotron radiation facilities, and we would like to thank Leonard Chavas and Christoph Mueller-Dieckmann for assistance in using beamlines Proxima 1 and ID30-B. We thank TechMedIII (ESBS, Illkirch, France) who carried out the pharmacokinetics experiments.

Appendix A. Supplementary material

Are present in supplementary material

References

- [1] World Health Organization, World malaria report 2018, 2018. <https://www.who.int/malaria/publications/world-malaria-report-2018/report/en/>.
- [2] A.M. Dondorp, F. Nosten, P. Yi, D. Das, A.P. Phyo, J. Tarning, K.M. Lwin, F. Arie, W. Hanpithakpong, S.J. Lee, P. Ringwald, K. Silamut, M. Imwong, K. Chotivanich, P. Lim, T. Herdman, S.S. An, S. Yeung, P. Singhasivanon, N.P.J. Day, N. Lindegardh, D. Socheat, N.J. White, Artemisinin Resistance in *Plasmodium falciparum* Malaria, *New England Journal of Medicine*. 361 (2009) 455–467. <https://doi.org/10.1056/NEJMoa0808859>.
- [3] M. Mishra, V. Singh, S. Singh, Structural Insights Into Key Plasmodium Proteases as Therapeutic Drug Targets, *Front. Microbiol.* 10 (2019). <https://doi.org/10.3389/fmicb.2019.00394>.
- [4] J. Liu, E.S. Istvan, I.Y. Gluzman, J. Gross, D.E. Goldberg, Plasmodium falciparum ensures its amino acid supply with multiple acquisition pathways and redundant proteolytic enzyme systems., *Proc Natl Acad Sci U S A.* 103 (2006) 8840–8845. <https://doi.org/10.1073/pnas.0601876103>.
- [5] D.A. Elliott, M.T. McIntosh, H.D. Hosgood, S. Chen, G. Zhang, P. Baevova, K.A. Joiner, Four distinct pathways of hemoglobin uptake in the malaria parasite Plasmodium falciparum, *PROC. NAT. ACAD. OF SCI. (U.S.A.)*. 105 (2008) 2463–2468. <https://doi.org/10.1073/pnas.0711067105>.
- [6] M. Krugliak, J. Zhang, H. Ginsburg, Intraerythrocytic Plasmodium falciparum utilizes only a fraction of the amino acids derived from the digestion of host cell cytosol for the biosynthesis of its proteins, *Molecular and Biochemical Parasitology*. 119 (2002) 249–256. [https://doi.org/10.1016/S0166-6851\(01\)00427-3](https://doi.org/10.1016/S0166-6851(01)00427-3).
- [7] D.E. Goldberg, Hemoglobin Degradation, in: R.W. Compans, M.D. Cooper, T. Honjo, H. Koprowski, F. Melchers, M.B.A. Oldstone, S. Olsnes, M. Potter, P.K. Vogt, H. Wagner, D.J. Sullivan, S. Krishna (Eds.), *Malaria: Drugs, Disease and Post-Genomic Biology*, Springer, Berlin, Heidelberg, 2005: pp. 275–291. https://doi.org/10.1007/3-540-29088-5_11.
- [8] V.L. Lew, T. Tiffert, H. Ginsburg, Excess hemoglobin digestion and the osmotic stability of Plasmodium falciparum–infected red blood cells, *Blood*. 101 (2003) 4189–4194. <https://doi.org/10.1182/blood-2002-08-2654>.
- [9] V.L. Lew, L. Macdonald, H. Ginsburg, M. Krugliak, T. Tiffert, Excess haemoglobin digestion by malaria parasites: a strategy to prevent premature host cell lysis, *Blood Cells, Molecules, and Diseases*. 32 (2004) 353–359. <https://doi.org/10.1016/j.bcmed.2004.01.006>.

- [10] M.B. Harbut, G. Velmourougane, S. Dalal, G. Reiss, J.C. Whisstock, O. Onder, D. Brisson, S. McGowan, M. Klemba, D.C. Greenbaum, Bestatin-based chemical biology strategy reveals distinct roles for malaria M1- and M17-family aminopeptidases, *PNAS*. 108 (2011) E526–E534. <https://doi.org/10.1073/pnas.1105601108>.
- [11] O. Azimzadeh, C. Sow, M. Gèze, J. Nyalwidhe, I. Florent, *Plasmodium falciparum* PfA-M1 aminopeptidase is trafficked via the parasitophorous vacuole and marginally delivered to the food vacuole, *Malaria Journal*. 9 (2010) 189. <https://doi.org/10.1186/1475-2875-9-189>.
- [12] M. Allary, J. Schrevel, I. Florent, Properties, stage-dependent expression and localization of *Plasmodium falciparum* M1 family zinc-aminopeptidase, *Parasitology*. 125 (2002). <https://doi.org/10.1017/S0031182002001828>.
- [13] D. Ragheb, S. Dalal, K.M. Bompiani, W.K. Ray, M. Klemba, Distribution and Biochemical Properties of an M1-family Aminopeptidase in *Plasmodium falciparum* Indicate a Role in Vacuolar Hemoglobin Catabolism, *J. Biol. Chem.* 286 (2011) 27255–27265. <https://doi.org/10.1074/jbc.M111.225318>.
- [14] A. Kitjaroenthom, T. Suthiphongchai, P. Wilairat, Effect of metalloprotease inhibitors on invasion of red blood cell by *Plasmodium falciparum*, *Acta Tropica*. 97 (2006) 5–9. <https://doi.org/10.1016/j.actatropica.2005.05.015>.
- [15] I. Florent, Z. Derhy, M. Allary, M. Monsigny, R. Mayer, J. Schrével, A *Plasmodium falciparum* aminopeptidase gene belonging to the M1 family of zinc-metalloproteases is expressed in erythrocytic stages, *Molecular and Biochemical Parasitology*. 97 (1998) 149–160. [https://doi.org/10.1016/S0166-6851\(98\)00143-1](https://doi.org/10.1016/S0166-6851(98)00143-1).
- [16] M.F. Nankya-Kitaka, G.P. Curley, C.S. Gavigan, A. Bell, J.P. Dalton, *Plasmodium chabaudi chabaudi* and *P. falciparum*: inhibition of aminopeptidase and parasite growth by bestatin and nitrobestatin, *Parasitol Res.* 84 (1998) 552–558. <https://doi.org/10.1007/s004360050447>.
- [17] C.S. Gavigan, J.P. Dalton, A. Bell, The role of aminopeptidases in haemoglobin degradation in *Plasmodium falciparum*-infected erythrocytes, *Molecular and Biochemical Parasitology*. 117 (2001) 37–48. [https://doi.org/10.1016/S0166-6851\(01\)00327-9](https://doi.org/10.1016/S0166-6851(01)00327-9).
- [18] S. Dalal, M. Klemba, Roles for Two Aminopeptidases in Vacuolar Hemoglobin Catabolism in *Plasmodium falciparum*, *J. Biol. Chem.* 282 (2007) 35978–35987. <https://doi.org/10.1074/jbc.M703643200>.
- [19] K. R. Trenholme, C. L. Brown, T. S. Skinner-Adams, C. Stack, J. Lowther, J. To, M. W. Robinson, S. M. Donnelly, J. P. Dalton, D. L. Gardiner, Aminopeptidases of Malaria Parasites: New Targets for Chemotherapy, *IDDT*. 10 (2010) 217–225. <https://doi.org/10.2174/187152610791163363>.
- [20] M.J. Gardner, N. Hall, E. Fung, O. White, M. Berriman, R.W. Hyman, J.M. Carlton, A. Pain, K.E. Nelson, S. Bowman, I.T. Paulsen, K. James, J.A. Eisen, K. Rutherford, S.L. Salzberg, A. Craig, S. Kyes, M.-S. Chan, V. Nene, S.J. Shallom, B. Suh, J. Peterson, S. Angiuoli, M. Pertea, J. Allen, J. Selengut, D. Haft, M.W. Mather, A.B. Vaidya, D.M.A. Martin, A.H. Fairlamb, M.J. Fraunholz, D.S. Roos, S.A. Ralph, G.I. McFadden, L.M. Cummings, G.M. Subramanian, C. Mungall, J.C. Venter, D.J. Carucci, S.L. Hoffman, C. Newbold, R.W. Davis, C.M. Fraser, B. Barrell, Genome sequence of the human malaria parasite *Plasmodium falciparum*, *Nature*. 419 (2002) 498–511. <https://doi.org/10.1038/nature01097>.
- [21] C. Aurrecochea, J. Brestelli, B.P. Brunk, J. Dommer, S. Fischer, B. Gajria, X. Gao, A. Gingle, G. Grant, O.S. Harb, M. Heiges, F. Innamorato, J. Iodice, J.C. Kissinger, E. Kraemer, W. Li, J.A. Miller, V. Nayak, C. Pennington, D.F. Pinney, D.S. Roos, C. Ross, C.J. Stoeckert, C. Treatman, H. Wang, PlasmoDB: a functional genomic database for malaria parasites, *Nucleic Acids Res.* 37 (2009) D539–D543. <https://doi.org/10.1093/nar/gkn814>.
- [22] R. Banerjee, J. Liu, W. Beatty, L. Pelosof, M. Klemba, D.E. Goldberg, Four plasmepsins are active in the *Plasmodium falciparum* food vacuole, including a protease with an active-site histidine, *PNAS*. 99 (2002) 990–995. <https://doi.org/10.1073/pnas.022630099>.
- [23] P. Grellier, D. Depoix, J. Schrével, I. Florent, Discovery of new targets for antimalarial chemotherapy, *Parasite*. 15 (2008) 219–225. <https://doi.org/10.1051/parasite/2008153219>.

- [24] T.S. Skinner-Adams, J. Lowther, F. Teuscher, C.M. Stack, J. Grembecka, A. Mucha, P. Kafarski, K.R. Trenholme, J.P. Dalton, D.L. Gardiner, Identification of Phosphinate Dipeptide Analog Inhibitors Directed against the Plasmodium falciparum M17 Leucine Aminopeptidase as Lead Antimalarial Compounds, *J. Med. Chem.* 50 (2007) 6024–6031. <https://doi.org/10.1021/jm070733v>.
- [25] M. Klemba, I. Gluzman, D.E. Goldberg, A Plasmodium falciparum Dipeptidyl Aminopeptidase I Participates in Vacuolar Hemoglobin Degradation, *J. Biol. Chem.* 279 (2004) 43000–43007. <https://doi.org/10.1074/jbc.M408123200>.
- [26] J. Lin, R. Spaccapelo, E. Schwarzer, M. Sajid, T. Annoura, K. Deroost, R.B.G. Ravelli, E. Aime, B. Capuccini, A.M. Mommaas-Kienhuis, T. O'Toole, F. Prins, B.M.D. Franke-Fayard, J. Ramesar, S. Chevalley-Maurel, H. Kroeze, A.J. Koster, H.J. Tanke, A. Crisanti, J. Langhorne, P. Arese, P.E. Van den Steen, C.J. Janse, S.M. Khan, Replication of Plasmodium in reticulocytes can occur without hemozoin formation, resulting in chloroquine resistance, *J Exp Med.* 212 (2015) 893–903. <https://doi.org/10.1084/jem.20141731>.
- [27] T. Weißbach, A. Golzmann, S. Bennink, G. Pradel, C. Julius Ngwa, Transcript and protein expression analysis of proteases in the blood stages of Plasmodium falciparum, *Experimental Parasitology.* 180 (2017) 33–44. <https://doi.org/10.1016/j.exppara.2017.03.006>.
- [28] L. Florens, M.P. Washburn, J.D. Raine, R.M. Anthony, M. Grainger, J.D. Haynes, J.K. Moch, N. Muster, J.B. Sacci, D.L. Tabb, A.A. Witney, D. Wolters, Y. Wu, M.J. Gardner, A.A. Holder, R.E. Sinden, J.R. Yates, D.J. Carucci, A proteomic view of the Plasmodium falciparum life cycle, *Nature.* 419 (2002) 520–526. <https://doi.org/10.1038/nature01107>.
- [29] E. Lasonder, C.J. Janse, G.-J. van Gemert, G.R. Mair, A.M.W. Vermunt, B.G. Douradinha, V. van Noort, M.A. Huynen, A.J.F. Luty, H. Kroeze, S.M. Khan, R.W. Sauerwein, A.P. Waters, M. Mann, H.G. Stunnenberg, Proteomic Profiling of Plasmodium Sporozoite Maturation Identifies New Proteins Essential for Parasite Development and Infectivity, *PLOS Pathogens.* 4 (2008) e1000195. <https://doi.org/10.1371/journal.ppat.1000195>.
- [30] F. Silvestrini, E. Lasonder, A. Olivieri, G. Camarda, B. van Schaijk, M. Sanchez, S.Y. Younis, R. Sauerwein, P. Alano, Protein Export Marks the Early Phase of Gametocytogenesis of the Human Malaria Parasite Plasmodium falciparum, *Molecular & Cellular Proteomics.* 9 (2010) 1437–1448. <https://doi.org/10.1074/mcp.M900479-MCP200>.
- [31] L. Florens, X. Liu, Y. Wang, S. Yang, O. Schwartz, M. Peglar, D.J. Carucci, J.R. Yates, Y. Wu, Proteomics approach reveals novel proteins on the surface of malaria-infected erythrocytes, *Molecular and Biochemical Parasitology.* 135 (2004) 1–11. <https://doi.org/10.1016/j.molbiopara.2003.12.007>.
- [32] N. Hall, A Comprehensive Survey of the Plasmodium Life Cycle by Genomic, Transcriptomic, and Proteomic Analyses, *Science.* 307 (2005) 82–86. <https://doi.org/10.1126/science.1103717>.
- [33] E. Lasonder, Y. Ishihama, J.S. Andersen, A.M.W. Vermunt, A. Pain, R.W. Sauerwein, W.M.C. Eling, N. Hall, A.P. Waters, H.G. Stunnenberg, M. Mann, Analysis of the Plasmodium falciparum proteome by high-accuracy mass spectrometry, *Nature.* 419 (2002) 537–542. <https://doi.org/10.1038/nature01111>.
- [34] S.E. Lindner, K.E. Swearingen, A. Harupa, A.M. Vaughan, P. Sinnis, R.L. Moritz, S.H.I. Kappe, Total and Putative Surface Proteomics of Malaria Parasite Salivary Gland Sporozoites, *Molecular & Cellular Proteomics.* 12 (2013) 1127–1143. <https://doi.org/10.1074/mcp.M112.024505>.
- [35] M. Lamarque, C. Tastet, J. Poncet, E. Demettré, P. Jouin, H. Vial, J.-F. Dubremetz, Food vacuole proteome of the malarial parasite Plasmodium falciparum, *PROTEOMICS – Clinical Applications.* 2 (2008) 1361–1374. <https://doi.org/10.1002/prca.200700112>.
- [36] J. Gonzalez-Bacero, R. Fando, A. del Monte-Martinez, J.-L. Charli, M. de los Angeles Chavez, Plasmodium falciparum M1-Aminopeptidase: A Promising Target for the Development of Antimalarials, *Current Drug Targets.* 15 (2014) 1144–1165. <https://doi.org/10.2174/1389450115666141024115641>.
- [37] T.S. Skinner-Adams, C.M. Stack, K.R. Trenholme, C.L. Brown, J. Grembecka, J. Lowther, A. Mucha, M. Drag, P. Kafarski, S. McGowan, J.C. Whisstock, D.L. Gardiner, J.P. Dalton,

- Plasmodium falciparum neutral aminopeptidases: new targets for anti-malarials, Trends in Biochemical Sciences. 35 (2010) 53–61. <https://doi.org/10.1016/j.tibs.2009.08.004>.
- [38] S. McGowan, C.J. Porter, J. Lowther, C.M. Stack, S.J. Golding, T.S. Skinner-Adams, K.R. Trenholme, F. Teuscher, S.M. Donnelly, J. Grembecka, A. Mucha, P. Kafarski, R. DeGori, A.M. Buckle, D.L. Gardiner, J.C. Whisstock, J.P. Dalton, Structural basis for the inhibition of the essential *Plasmodium falciparum* M1 neutral aminopeptidase, Proceedings of the National Academy of Sciences. 106 (2009) 2537–2542. <https://doi.org/10.1073/pnas.0807398106>.
- [39] T.S. Skinner-Adams, C.L. Peatey, K. Anderson, K.R. Trenholme, D. Krige, C.L. Brown, C. Stack, D.M.M. Nsangou, R.T. Mathews, K. Thivierge, J.P. Dalton, D.L. Gardiner, The Aminopeptidase Inhibitor CHR-2863 Is an Orally Bioavailable Inhibitor of Murine Malaria, Antimicrobial Agents and Chemotherapy. 56 (2012) 3244–3249. <https://doi.org/10.1128/AAC.06245-11>.
- [40] E. Zervoudi, A. Papakyriakou, D. Georgiadou, I. Evnouchidou, A. Gajda, M. Poreba, G.S. Salvesen, M. Drag, A. Hattori, L. Swevers, D. Vourloumis, E. Stratikos, Probing the S1 specificity pocket of the aminopeptidases that generate antigenic peptides, Biochemical Journal. 435 (2011) 411–420. <https://doi.org/10.1042/BJ20102049>.
- [41] C.M. Stack, J. Lowther, E. Cunningham, S. Donnelly, D.L. Gardiner, K.R. Trenholme, T.S. Skinner-Adams, F. Teuscher, J. Grembecka, A. Mucha, P. Kafarski, L. Lua, A. Bell, J.P. Dalton, Characterization of the Plasmodium falciparum M17 Leucyl Aminopeptidase a protease involved in amino acid regulation with potential for antimalarial drug development, J. Biol. Chem. 282 (2007) 2069–2080. <https://doi.org/10.1074/jbc.M609251200>.
- [42] S. Albrecht, M. Al-Lakkis-Wehbe, A. Orsini, A. Defoin, P. Pale, E. Salomon, C. Tarnus, J.-M. Weibel, Amino-benzosuberone: A novel warhead for selective inhibition of human aminopeptidase-N/CD13, Bioorganic & Medicinal Chemistry. 19 (2011) 1434–1449. <https://doi.org/10.1016/j.bmc.2011.01.008>.
- [43] C. Maieranu, C. Schmitt, N. Schifano-Faux, D. Le Nouën, A. Defoin, C. Tarnus, A novel amino-benzosuberone derivative is a picomolar inhibitor of mammalian aminopeptidase N/CD13, Bioorganic & Medicinal Chemistry. 19 (2011) 5716–5733. <https://doi.org/10.1016/j.bmc.2011.06.089>.
- [44] C. Schmitt, M. Voegelin, A. Marin, M. Schmitt, F. Schegg, P. Hénon, D. Guenot, C. Tarnus, Selective aminopeptidase-N (CD13) inhibitors with relevance to cancer chemotherapy, Bioorganic & Medicinal Chemistry. 21 (2013) 2135–2144. <https://doi.org/10.1016/j.bmc.2012.12.038>.
- [45] R. Pasqualini, E. Koivunen, R. Kain, J. Lahdenranta, M. Sakamoto, A. Stryhn, R.A. Ashmun, L.H. Shapiro, W. Arap, E. Ruoslahti, Aminopeptidase N is a Receptor for Tumor-homing Peptides and a Target for Inhibiting Angiogenesis, Cancer Res. 60 (2000) 722–727.
- [46] P. Mina-Osorio, The moonlighting enzyme CD13: old and new functions to target, Trends in Molecular Medicine. 14 (2008) 361–371. <https://doi.org/10.1016/j.molmed.2008.06.003>.
- [47] E. Salomon, M. Schmitt, A. Marapaka, A. Stamogiannos, G. Revelant, C. Schmitt, S. Alavi, I. Florent, A. Addlagatta, E. Stratikos, C. Tarnus, S. Albrecht, E. Salomon, M. Schmitt, A.K. Marapaka, A. Stamogiannos, G. Revelant, C. Schmitt, S. Alavi, I. Florent, A. Addlagatta, E. Stratikos, C. Tarnus, S. Albrecht, Aminobenzosuberone Scaffold as a Modular Chemical Tool for the Inhibition of Therapeutically Relevant M1 Aminopeptidases, Molecules. 23 (2018) 2607. <https://doi.org/10.3390/molecules23102607>.
- [48] L. Bounaadja, M. Schmitt, S. Albrecht, E. Mouray, C. Tarnus, I. Florent, Selective inhibition of PfA-M1, over PfA-M17, by an amino-benzosuberone derivative blocks malaria parasites development in vitro and in vivo, Malaria Journal. 16 (2017). <https://doi.org/10.1186/s12936-017-2032-4>.
- [49] G. Velmourougane, M.B. Harbut, S. Dalal, S. McGowan, C.A. Oellig, N. Meinhardt, J.C. Whisstock, M. Klemba, D.C. Greenbaum, Synthesis of New (–)-Bestatin-Based Inhibitor Libraries Reveals a Novel Binding Mode in the S1 Pocket of the Essential Malaria M1 Metalloaminopeptidase, J. Med. Chem. 54 (2011) 1655–1666. <https://doi.org/10.1021/jm101227t>.

- [50] M. Flipo, T. Beghyn, V. Leroux, I. Florent, B.P. Deprez, R.F. Deprez-Poulain, Novel Selective Inhibitors of the Zinc Plasmodial Aminopeptidase PfA-M1 as Potential Antimalarial Agents, *J. Med. Chem.* 50 (2007) 1322–1334. <https://doi.org/10.1021/jm061169b>.
- [51] R. Deprez-Poulain, M. Flipo, C. Piveteau, F. Leroux, S. Dassonneville, I. Florent, L. Maes, P. Cos, B. Deprez, Structure–Activity Relationships and Blood Distribution of Antiplasmodial Aminopeptidase-1 Inhibitors, *J. Med. Chem.* 55 (2012) 10909–10917. <https://doi.org/10.1021/jm301506h>.
- [52] S.N. Mistry, N. Drinkwater, C. Ruggeri, K.K. Sivaraman, S. Loganathan, S. Fletcher, M. Drag, A. Paiardini, V.M. Avery, P.J. Scammells, S. McGowan, Two-Pronged Attack: Dual Inhibition of Plasmodium falciparum M1 and M17 Metalloaminopeptidases by a Novel Series of Hydroxamic Acid-Based Inhibitors, *J. Med. Chem.* 57 (2014) 9168–9183. <https://doi.org/10.1021/jm501323a>.
- [53] N. Drinkwater, N.B. Vinh, S.N. Mistry, R.S. Bamert, C. Ruggeri, J.P. Holleran, S. Loganathan, A. Paiardini, S.A. Charman, A.K. Powell, V.M. Avery, S. McGowan, P.J. Scammells, Potent dual inhibitors of Plasmodium falciparum M1 and M17 aminopeptidases through optimization of S1 pocket interactions, *European Journal of Medicinal Chemistry.* 110 (2016) 43–64. <https://doi.org/10.1016/j.ejmech.2016.01.015>.
- [54] N.B. Vinh, N. Drinkwater, T.R. Malcolm, M. Kassiou, L. Lucantoni, P.M. Grin, G.S. Butler, S. Duffy, C.M. Overall, V.M. Avery, P.J. Scammells, S. McGowan, Hydroxamic Acid Inhibitors Provide Cross-Species Inhibition of Plasmodium M1 and M17 Aminopeptidases, *J. Med. Chem.* 62 (2019) 622–640. <https://doi.org/10.1021/acs.jmedchem.8b01310>.
- [55] J. González-Bacerio, S.E.C. Maluf, Y. Méndez, I. Pascual, I. Florent, P.M.S. Melo, A. Budu, J.C. Ferreira, E. Moreno, A.K. Carmona, D.G. Rivera, M. Alonso del Rivero, M.L. Gazarini, KBE009: An antimalarial bestatin-like inhibitor of the Plasmodium falciparum M1 aminopeptidase discovered in an Ugi multicomponent reaction-derived peptidomimetic library, *Bioorganic & Medicinal Chemistry.* 25 (2017) 4628–4636. <https://doi.org/10.1016/j.bmc.2017.06.047>.
- [56] D. Osella, M. Ferrali, P. Zanello, F. Laschi, M. Fontani, C. Nervi, G. Cavigiolio, On the mechanism of the antitumor activity of ferrocenium derivatives, *Inorganica Chimica Acta.* 306 (2000) 42–48. [https://doi.org/10.1016/S0020-1693\(00\)00147-X](https://doi.org/10.1016/S0020-1693(00)00147-X).
- [57] N. Chavain, H. Vezin, D. Dive, N. Touati, J.-F. Paul, E. Buisine, C. Biot, Investigation of the Redox Behavior of Ferroquine, a New Antimalarial, *Mol. Pharmaceutics.* 5 (2008) 710–716. <https://doi.org/10.1021/mp800007x>.
- [58] M. Bartošík, L. Koubková, J. Karban, L. Červenková Šťastná, T. Hodík, M. Lamač, J. Pinkas, R. Hrstka, Electrochemical analysis of a novel ferrocene derivative as a potential antitumor drug, *Analyst.* 140 (2015) 5864–5867. <https://doi.org/10.1039/C5AN00958H>.
- [59] B.H. Neufeld, J.B. Tapia, A. Lutzke, M.M. Reynolds, Small Molecule Interferences in Resazurin and MTT-Based Metabolic Assays in the Absence of Cells, *Anal. Chem.* 90 (2018) 6867–6876. <https://doi.org/10.1021/acs.analchem.8b01043>.
- [60] P.A. Karplus, K. Diederichs, Assessing and maximizing data quality in macromolecular crystallography, *Current Opinion in Structural Biology.* 34 (2015) 60–68. <https://doi.org/10.1016/j.sbi.2015.07.003>.
- [61] G. Peng, A.G. McEwen, V. Olieric, C. Schmitt, S. Albrecht, J. Cavarelli, C. Tarnus, Insight into the remarkable affinity and selectivity of the aminobenzosuberone scaffold for the M1 aminopeptidases family based on structure analysis, *Proteins: Structure, Function, and Bioinformatics.* 85 (2017) 1413–1421. <https://doi.org/10.1002/prot.25301>.
- [62] W. Trager, J.B. Jensen, Human malaria parasites in continuous culture, *Science.* 193 (1976) 673–675. <https://doi.org/10.1126/science.781840>.
- [63] R.E. Desjardins, C.J. Canfield, J.D. Haynes, J.D. Chulay, Quantitative assessment of antimalarial activity in vitro by a semiautomated microdilution technique., *Antimicrobial Agents and Chemotherapy.* 16 (1979) 710–718. <https://doi.org/10.1128/AAC.16.6.710>.
- [64] J. Gabadinho, A. Beteva, M. Guijarro, V. Rey-Bakaikoa, D. Spruce, M.W. Bowler, S. Brockhauser, D. Flot, E.J. Gordon, D.R. Hall, B. Lavault, A.A. McCarthy, J. McCarthy, E. Mitchell, S. Monaco, C.

- Mueller-Dieckmann, D. Nurizzo, R.B.G. Ravelli, X. Thibault, M.A. Walsh, G.A. Leonard, S.M. McSweeney, MxCuBE: a synchrotron beamline control environment customized for macromolecular crystallography experiments, *J Synchrotron Rad.* 17 (2010) 700–707. <https://doi.org/10.1107/S0909049510020005>.
- [65] W. Kabsch, XDS, *Acta Crystallogr D Biol Crystallogr.* 66 (2010) 125–132. <https://doi.org/10.1107/S0907444909047337>.
- [66] P. Evans, Scaling and assessment of data quality, *Acta Cryst D.* 62 (2006) 72–82. <https://doi.org/10.1107/S0907444905036693>.
- [67] P.R. Evans, An introduction to data reduction: space-group determination, scaling and intensity statistics, *Acta Cryst D.* 67 (2011) 282–292. <https://doi.org/10.1107/S090744491003982X>.
- [68] M.D. Winn, C.C. Ballard, K.D. Cowtan, E.J. Dodson, P. Emsley, P.R. Evans, R.M. Keegan, E.B. Krissinel, A.G.W. Leslie, A. McCoy, S.J. McNicholas, G.N. Murshudov, N.S. Pannu, E.A. Potterton, H.R. Powell, R.J. Read, A. Vagin, K.S. Wilson, Overview of the CCP4 suite and current developments, *Acta Cryst D.* 67 (2011) 235–242. <https://doi.org/10.1107/S0907444910045749>.
- [69] A.J. McCoy, R.W. Grosse-Kunstleve, P.D. Adams, M.D. Winn, L.C. Storoni, R.J. Read, Phaser crystallographic software, *J Appl Crystallogr.* 40 (2007) 658–674. <https://doi.org/10.1107/S0021889807021206>.
- [70] P.D. Adams, P.V. Afonine, G. Bunkóczi, V.B. Chen, I.W. Davis, N. Echols, J.J. Headd, L.-W. Hung, G.J. Kapral, R.W. Grosse-Kunstleve, A.J. McCoy, N.W. Moriarty, R. Oeffner, R.J. Read, D.C. Richardson, J.S. Richardson, T.C. Terwilliger, P.H. Zwart, PHENIX: a comprehensive Python-based system for macromolecular structure solution, *Acta Cryst D.* 66 (2010) 213–221. <https://doi.org/10.1107/S0907444909052925>.
- [71] N. Drinkwater, R.S. Bamert, K.K. Sivaraman, A. Paiardini, S. McGowan, X-ray crystal structures of an orally available aminopeptidase inhibitor, Tosedostat, bound to anti-malarial drug targets *Pf* A-M1 and *Pf* A-M17: Structures of *Pf* A-M1/M17 Bound to Tosedostat, *Proteins: Structure, Function, and Bioinformatics.* 83 (2015) 789–795. <https://doi.org/10.1002/prot.24771>.
- [72] B.W. Matthews, Solvent content of protein crystals, *Journal of Molecular Biology.* 33 (1968) 491–497. [https://doi.org/10.1016/0022-2836\(68\)90205-2](https://doi.org/10.1016/0022-2836(68)90205-2).
- [73] P.V. Afonine, R.W. Grosse-Kunstleve, N. Echols, J.J. Headd, N.W. Moriarty, M. Mustyakimov, T.C. Terwilliger, A. Urzhumtsev, P.H. Zwart, P.D. Adams, Towards automated crystallographic structure refinement with phenix.refine, *Acta Cryst D.* 68 (2012) 352–367. <https://doi.org/10.1107/S0907444912001308>.
- [74] P. Emsley, B. Lohkamp, W.G. Scott, K. Cowtan, Features and development of Coot, *Acta Cryst D.* 66 (2010) 486–501. <https://doi.org/10.1107/S0907444910007493>.
- [75] C.J. Williams, J.J. Headd, N.W. Moriarty, M.G. Prisant, L.L. Videau, L.N. Deis, V. Verma, D.A. Keedy, B.J. Hintze, V.B. Chen, S. Jain, S.M. Lewis, W.B. Arendall, J. Snoeyink, P.D. Adams, S.C. Lovell, J.S. Richardson, D.C. Richardson, MolProbity: More and better reference data for improved all-atom structure validation, *Protein Science.* 27 (2018) 293–315. <https://doi.org/10.1002/pro.3330>.
- [76] Y. Zhang, M. Huo, J. Zhou, S. Xie, PKSolver: An add-in program for pharmacokinetic and pharmacodynamic data analysis in Microsoft Excel, *Computer Methods and Programs in Biomedicine.* 99 (2010) 306–314. <https://doi.org/10.1016/j.cmpb.2010.01.007>.
-